



Gold-black as IR absorber and solar cell enhancer

Journal:	<i>2009 MRS Fall Meeting</i>
Manuscript ID:	Draft
Symposium:	Symposium O
Date Submitted by the Author:	
Complete List of Authors:	Peale, Robert; University of Central Florida Cleary, Justin; University of Central Florida, Physics Ishigami, Masahito; University of Central Florida, Physics Smith, Christian; University of Central Florida, Physics Baillie, Kevin; University of Central Florida, Physics Colwell, Josh; University of Central Florida, Physics Beck, Kenneth; Pacific Northwest Nat Lab, EMSL Edwards, Oliver; Pacific Northwest Nat Lab, EMSL Fredricksen, Chris; LRC Engineering Inc.
Keywords:	photoemission, infrared (IR) spectroscopy, Au



Gold-black as IR absorber and solar cell enhancer

R. E. Peale¹, J. W. Cleary¹, M. Ishigami¹, C. W. Smith¹, K. Baillie¹, J. E. Colwell¹, K. M. Beck², A. G. Joly², O. Edwards³, C. J. Fredricksen⁴

¹Department of Physics, University of Central Florida, Orlando FL 32816

²Pacific Northwest National Laboratory, William R. Wiley Environmental Molecular Science Laboratory, Richland, WA 99352

³Zyberwear, Inc., 2114 New Victor Road, Ocoee FL 34761

⁴LRC Engineering, Inc., 9345 Chandon Dr., Orlando FL 32825

ABSTRACT

Infrared absorbance and visible/near-IR excited plasmon resonances are investigated in gold-black, a porous nano-structured conducting film. Polymer infusion (for hardening) generally reduced absorbance in the long wave IR but has little effect at THz wavelengths. The characteristic length scales of the structured films vary considerably as a function of deposition parameters, but the absorbance is found to be only weakly correlated with these distributions. Initial investigations of gold-black by photoelectron emission microscopy (PEEM) reveal plasmon resonances, which have potential to enhance the efficiency of thin film solar cells. For films with different characteristic length scales, the plasmon resonances appear in structures with similar length scales.

INTRODUCTION

Metal-black nano-structured conducting films have been exploited as broad-band surface absorbers for bolometers [1-3]. This paper considers the effect for this application of hardening of gold-black via polymer infusion and the possible correlation of IR absorption to the characteristic length scales of the films. Also presented are initial investigations of the plasmon resonance characteristics of gold-black, which has potential to increase the efficiency of thin film solar cells via resonant scattering and field enhancement.

Metal blacks have been investigated for their optical properties since the 1930's [4]. Deposition by evaporation in an inert gas at tenths to tens of Torr has followed the method of Harris [5-9] with little change. One objective of this work was to develop an absorber for an innovative MEMS-based bolometric infrared imaging array detector with high frame rates. Metal blacks are produced in a low-vacuum process, resulting in a porous nano-structured metallic film having a broad particle-size distribution. The morphology depends on the pressure of the inert gas in the evaporation chamber, the deposition rate, and the temperature of the substrate [5]. A correlation between the absorptivity of gold black and the resistivity of the thin films has been exploited [10] to verify the expected properties of as-grown films. Here the possibility of a correlation between absorption and the particle size distribution is investigated.

Silicon has low absorption due to its indirect gap, such that usual solar cells require ~100 micron thickness to capture the incident solar irradiation, but thin films would be preferred for economy and weight. Small metal particles have potential to improve the efficiency of thin-film solar cells via the scattering and field enhancement. Photocurrent gains up to 10 x have been reported [11, 12]. Metallic scattering centers increase the effective optical path length in thin

films. The scattering cross section peaks at the plasmon resonance frequency, where there is also an enhancement in field strength. The resonance depends on particle size, an effect exploited for centuries to produce stained-glass windows. This paper reports initial investigations of particle size-dependence of optically-excited plasmon resonance in gold blacks.

EXPERIMENT

Gold-black is produced here by thermal evaporation in a chamber that has been back-filled with 1-2 Torr of inert gas, either nitrogen or helium. Initial experiments determined the parameters of interest and their useful ranges. Then, a two level full factorial optimization scheme, including polymer infusion, was followed to determine the conditions that produce maximum absorbance, giving samples in a series labeled “C”. Parameters chosen to be varied were He pressure, evaporation current, and substrate temperature. Each parameter took one of two values. In addition, after characterizing these samples, they were infused with polymer to two different levels of saturation. With 4 parameters, we have $2^4 = 16$ different combinations. Four intermediate points were also included to reveal curvature. A matrix of experiments was set up so that every combination of parameter values in the scheme is completed in random order to avoid systematic errors. The location in parameter space that optimized the films (as characterized by a figure of merit to be defined) and correlations between parameters are then discovered.

Infrared absorption was determined from transmittance and reflectance spectra collected using a BOMEM DA8 Fourier transform spectrometer. Transmittance used a clean silicon substrate as a reference. Specular reflectance at 30 deg angle of incidence was referenced to a gold-coated silicon substrate. The figure of merit (FOM) was defined as $1-T-R$, a measure of absorbance. It is not exactly the same as absorbance, however, since the reflectance was not at normal incidence.

Scanning electron microscope (SEM) images were collected on various instruments at UCF and EMSL. We performed a discrete wavelet analysis on each image using a Morlet wavelet [13,14]. We calculated the wavelet transform for each row of each image. The wavelet transform provides a map of the power present at all wavelengths at different regions of the image, or in this case at different locations within each image row. We integrated the wavelet power along the image row and then sum the power for all rows because we are interested in the overall wavelength power distribution, not spatial variations within the images.

PhotoElectron Emission Microscopy (PEEM) was used to characterize the spatial distribution of the plasmon resonances. PEEM used a near infrared laser (below the work function of gold (5.1 eV), or a Hg lamp, to excite plasmon resonances. A cooled CCD camera records photo-electron emission from the samples. The Hg arc lamp uses band-pass filters to cover the 400-800 nm range in 50 nm wide steps. Neutral density filters and a calibrated detector allowed us to control the photon fluence within each band.

RESULTS

Infrared FOM was determined at 100 and 650 cm^{-1} wavenumbers, corresponding roughly to the THz and long wave IR (LWIR) bands. The results are summarized in Fig. 1. The samples are numbered in the order they were prepared. The FOM values at 150 and 600 cm^{-1} are strongly correlated. A tendency of polymer infusion to reduce the FOM at 600 cm^{-1} is observed, but this is less significant at 150 cm^{-1} . For the samples with highest FOM there is a tendency for

polymer infusion to increase the figure of merit slightly. Mid-point measurements allow us to conclude that the dependence of FOM on each variable, and as well as interactions between variables, have strong curvature.

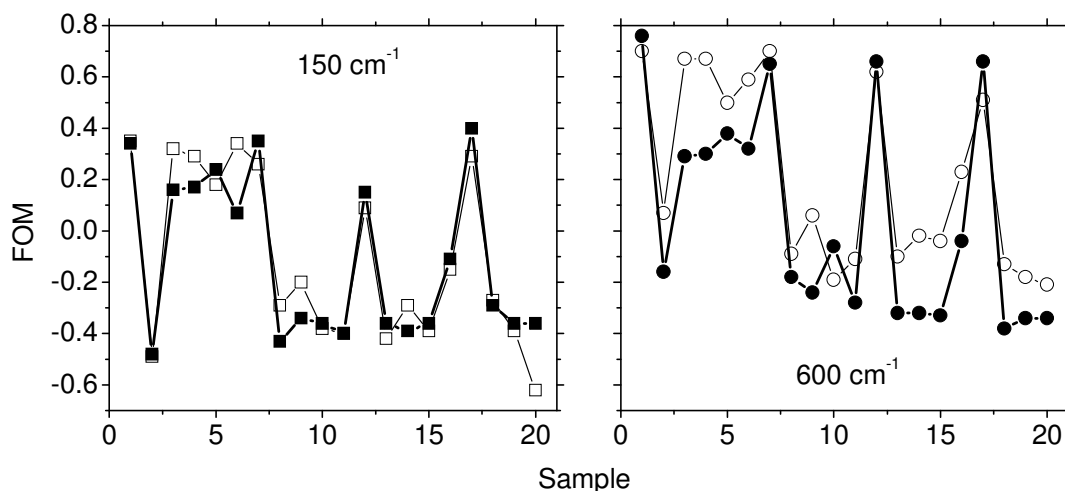


Fig. 1. Figures of merit at THz and Long-wave IR frequencies for gold-black samples of Table I. Solid (open) symbols indicate values after (before) polymer infusion.

Fig. 2 present SEM images of two of the gold black samples from Table I. The metallic particles are arranged in interconnected groups with a broad-range of characteristic length scales or spatial wavelengths. These two images were chosen for presentation because of the large difference in their characteristic length scales.

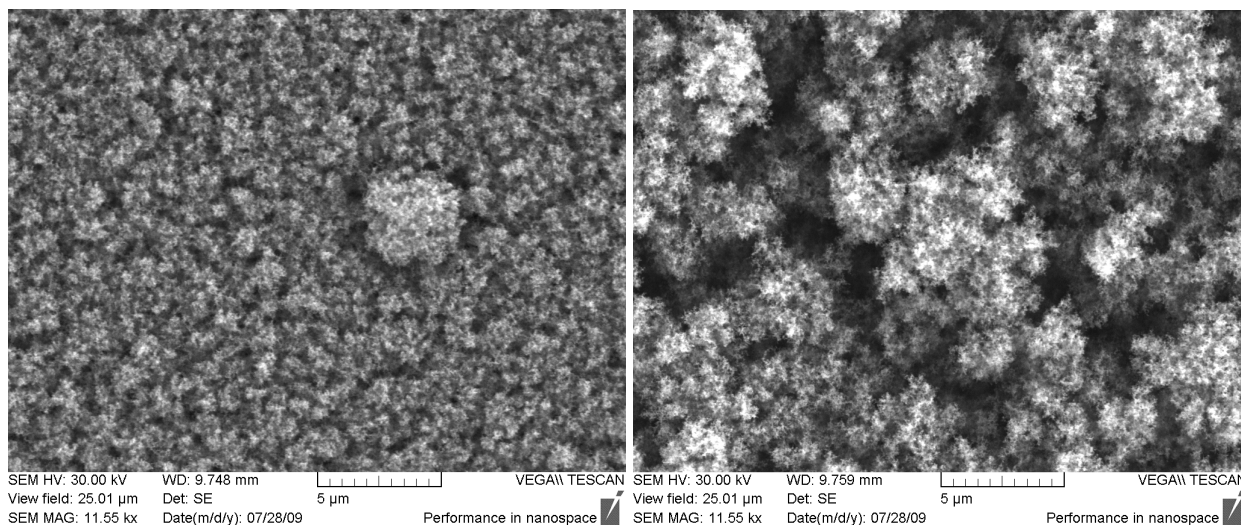


Fig. 2. SEM images of sample C04 (left) and C09 (right). Both images have 25 micron field of view.

Fig. 3 (left) presents the wavelet analysis of SEM images for C04 and C09 with 50 micron field of view. The wavelet power spectrum is characterized by a series of overlapping peaks. The upper wavelength cutoff is determined by the maximum dimension of the image. For two images with the same magnification, the lower limit is a quantitative measure of the

minimum characteristic length scale in the image. We define the minimum characteristic length scale as the point where the power is half the maximum value.

Fig. 3 (right) plots FOM values at THz and LWIR wavelengths as a function of the minimum length scale from the wavelet analysis of images with 50 micron FOV. At each wavelength, the FOM values appear in roughly two groups. Within each group there is no clear correlation between FOM and length scale. However considering both groups simultaneously, there appears to be a slight tendency for the high FOM points to be clustered at low length scale and vice versa. In other words, there may be a tendency for samples with smaller length scales to give higher absorbance.

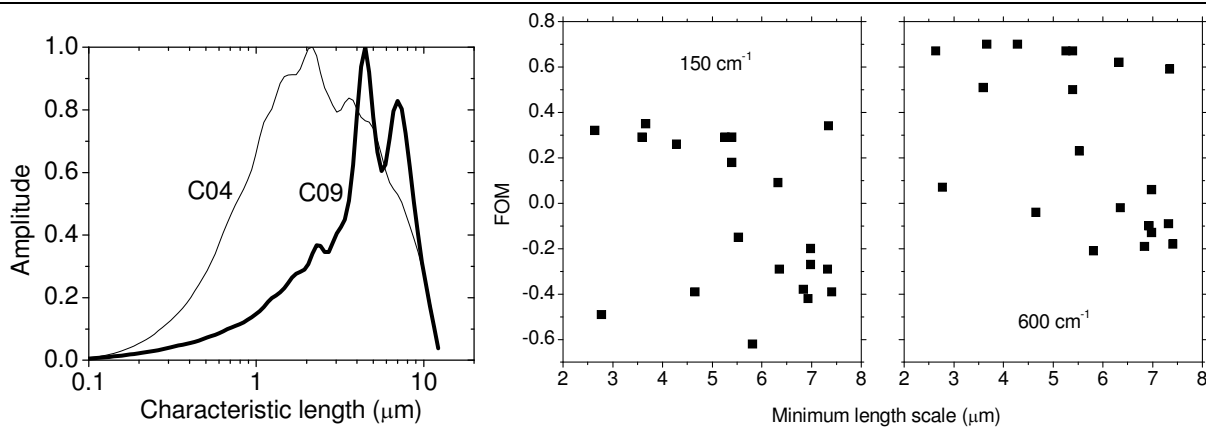


Fig. 3. (left) Wavelet analysis of SEM images for samples C04 and C09. The images had 50 micron field of view. The amplitude scale is normalized. (right) Infrared figure of merit as function of minimum characteristic length scale for gold-black.

Fig. 4 (left) presents PEEM images for Hg-arc-lamp illumination of samples C01, and C13. The image records the spatial position of emitted photoelectrons. The bright areas are “hot spots”, where plasmon resonances facilitate photoemission. These initial PEEM studies were on samples designed as IR absorbers. For plasmonic solar cell enhancement, the substrate coverage would need to be much lower. Still these observations give some indication of what effects one might expect. The lower left part of the sample C13 has been modified by a focused ion-beam mill (FIB) to make a marker for alignment. First, the modified surface has a noticeably different morphology in the SEM image and is less bright in the PEEM image, showing that it has less plasmon activity. Second, the distribution of bright-white hotspots in the PEEM image is less dense in the modified region than one might expect from the distribution of comparable structures in the SEM image. In principle, analysis of the histograms might be used to quantify the hot spot density.

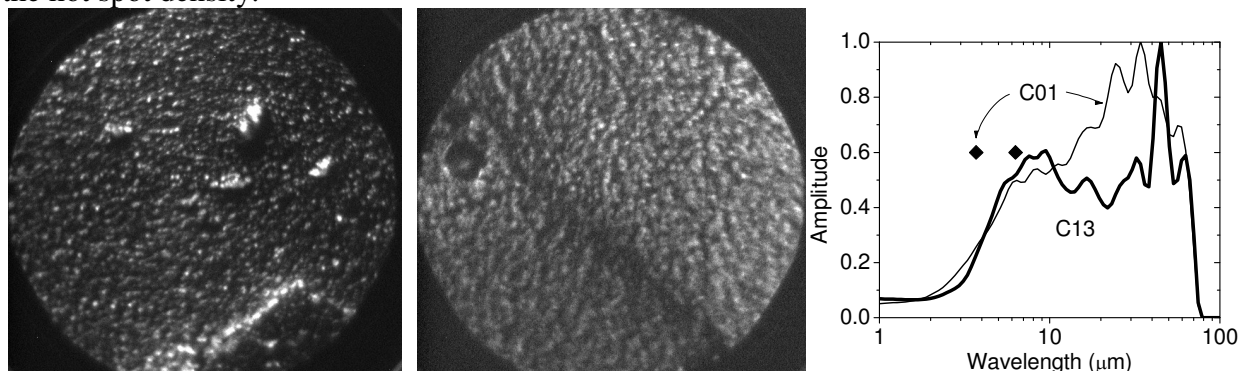


Fig. 4. (left) PEEM images of samples C01, and C13 (FOV = 150 microns.) (right) Wavelet analysis of the PEEM images. Symbols indicate the minimum length scale from SEM images.

Fig. 4 (right) presents wavelet analysis for the PEEM images of Fig. 4 (left). The symbols indicate the minimum length scale from the SEM images (50 micron FOV). We note that though the two samples have significantly different morphology and particle size distributions, the wavelet analysis shows that the plasmon resonances first appear at nearly the same length scale, namely at about 5 microns. This is true even though sample C13 has comparatively few structures as small as 5 microns. This size is comparable to the size of the hot spots in Fig. 4 (left). These results tentatively suggest that there is a certain preferred size for the excitation of plasmon resonances, and that this size may be larger (as in the case of C01) than the minimum size in the sample. Above this size, however, there is a broad range of length scales that give rise to plasmon-assisted photo-emission.

Fig. 5 presents preliminary wavelength dependence results. The field of view is 50 microns. The two laser wavelengths are not very different, and consequently, the hot-spot distribution for the two images is nearly identical. Nevertheless, the image for the longer wavelength shows more contrast, i.e. the hot-spots are brighter relative to the background. We suggest that this is because the wavelength is now closer to the surface plasmon resonance wavelength for gold (~500 nm).

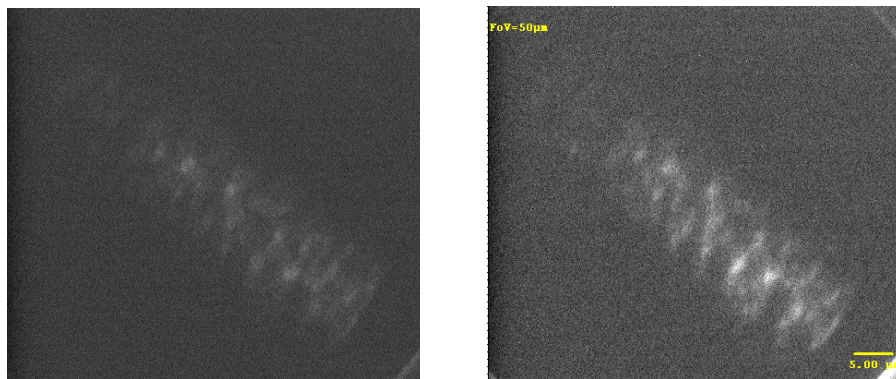


Fig. 5. PEEM image of gold black sample illuminated by a laser at (left) 370 and (right) 420 nm wavelength.

CONCLUSIONS

The results presented here suggest that hardening of gold black tends to lower the LWIR FOM somewhat, while this characteristic is less affected in the THz spectral range. Our hypothesis that the IR absorbance would be correlated with the characteristic length scale of the gold-black films is poorly supported by experiment. The observation of photoelectron emission from gold-black samples for wavelengths well below the work function of gold (5.1 eV) suggests that the emission occurs due to the field enhancement at the plasmon resonances. Thus, there is potential for similar useful effects in to enhance the efficiency of solar cells. That there is a broad range of length scales that contribute significantly to the plasmon-assisted photoemission

supports our suggestion that gold black may be a suitable material for plasmon-resonance enhancement of solar cell efficiency over the broad solar spectrum.

ACKNOWLEDGMENTS

REP and JWC are supported by a grant from AFOSR. Pacific Northwest National Laboratory is operated for the U.S. Department of Energy by Battelle. PEEM and some of the SEM experiments were performed in the Environmental Molecular Sciences Laboratory, a U.S. Department of Energy user facility operated by the office of Biological and Environmental Research. JEC and KB were supported by NASA's Cassini Data Analysis Program Grant NNX08AJ68G. The contributions of LRC Engineering were supported by an AFOSR Phase I STTR (John Hottle program manager).

REFERENCES

1. C. Doland, P. O'Neill, and A. Ignatiev, "*Particulate nature of solar absorbing films: Gold black*," J. Vac. Sci. Tech. **14** (1), 259-262, (1977).
2. P. O'Neill, C. Doland, and A. Ignatiev, "*Structural composition and optical properties of solar blacks: gold black*," Applied Optics **16** (11), 2822-2826, (1977).
3. N. Nelms and J. Dowson, "*Goldblack coating for thermal infrared detectors*," Sensors and Actuators A. **120**, 403-407, (2005).
4. A. H. Pfund, "*The Optical Properties of Metallic and Crystalline Powders*," J.O.S.A. **23**, 375-378, (1933).
5. L. Harris, R. T. McGinnies, and B. M. Siegel, "*The Preparation and Optical Properties of Gold Blacks*," J. Opt. Soc. Am. **38** (7), 582-589, (1948).
6. L. Harris and J. K. Beasley, "*The Infrared Properties of Gold Smoke Deposits*," J. Opt. Soc. Am. **42** (2), 134-140, (1952).
7. L. Harris and A. L. Loeb, "*Conductance and Relaxation Time of Electrons in Gold Blacks from Transmission and Reflection Measurements in the Far Infrared*," J. Opt. Soc. Am. **43** (11), 1114-1118, (1953).
8. L. Harris, "*The Transmittance and Reflectance of Gold Black Deposits in the 15- to 100-Micron Region*," J. Opt. Soc. Am. **51** (1), 80-82, (1961).
9. L. Harris and P. Fowler, "*Absorptance of Gold in the Far Infrared*," J. Opt. Soc. Am. **51** (2), 164-167, (1961).
10. W. Becker, R. Fettig, and W. Ruppel, "*Optical and electrical properties of black gold layers in the far infrared*," Infrared Phys. & Tech. **40**, 431-445, (1999).
11. H. R. Stuart D. G. Hall, "*Island size effects in nanoparticles-enhanced photodetectors*," App. Phys. Lett. **73** (26), 3815-3817 (1998).
12. K. R. Catchpole, S. Pillai, "*Absorption enhancement due to scattering by dipoles into silicon waveguides*," J. Appl. Phys. **100** (4), 044504 (2006).
13. G. Foster, "*Wavelets for period analysis of unevenly sampled time series*," Astron. J. **112**, 1709-1729 (1996).
14. C. Torrence, G. P. Compo, "*A practical guide to wavelet analysis*," Bull. Amer. Met. Soc. **79**, 61-78 (1998).